ChemistrySelect

Research Article
doi.org/10.1002/slct.202502878

Chemistry Europe
European Chemical Societies Publishing

www.chemistryselect.org

Catalyst-Free Synthesis of Quinazolinone-Fused Quinoxaline Derivatives under Mild Conditions: Characterization, In Silico Prediction and Biological Evaluation

Venkadachalam Rahimiya,[a] Mahesh Kalidasan,[b] Krishnamoorthy Bellie Sundaram,[c] and Appaswami Lalitha*[a]

Benzoyl indenoquinoxalines (BIQ) were synthesized by the cyclo-condensation of 3,4-diaminobenzophenone with 1,2-diketone derivatives in the presence of ethanol at room temperature. The reaction protocol is very simple that avoids toxic solvents and catalysts, resulting in a more environmentally friendly synthetic method. Using this method, quinoxaline derivatives as biologically potent molecules are formed with excellent yields in shorter reaction times. Benzoyl indenoquinoxalines synthesized were characterized by using FT-IR, NMR, and Mass spectral studies. The molecular structures of two selected benzoyl indenoquinoxalines were also confirmed by the single-crystal X-ray diffraction method. Moreover, molecular docking study of these compounds showed more effective binding with human epidermal growth factor receptor tyrosine kinase (4HJO). Theoretical calculations at the DFT (BP86/Def2-TZVP) level supported the experimental findings. The reactivity of the quinoxaline compounds was examined using the global reactivity descriptors and the frontier molecules orbitals (FMOs). The antimicrobial activities of the synthesized quinoxaline compounds against bacterial species such as *Streptococcus aureus, Escherichia coli*, and *Klebsiella pneumoniae* in different concentrations reveal notable responses depending on the strain and the concentration of the compounds examined.

1. Introduction

Heterocyclic compounds, especially the nitrogen-containing heterocycles have a wide-ranging of applications, in the fields of pharmaceutical,[1–4] agrochemicals, and natural products.[5] Quinoxalines, a class of *N*-heterocyclic compounds, have important biological applications, and industrial quinoxaline (C=N) compounds are the most important because, they are the backbone of a large variety of products such as intermediates for the preparation of new biologically active substances and also used in marketed drugs.[6,7] Owing to their excellent bioactivity, quinoxaline motifs remain the backbone of many fungicides, herbicides, and insecticides, and pharmaceutically important anticancer, anti-inflammatory, anticancer, antibacterial, antiviral, and antimalarial drugs.[8–11] The use of environmentally friendly conditions, such as catalyst-free, economical, easy to conduct experiments, easy to build up, and simple to recover, has gained popularity in the field of modern chemistry as it seeks to develop more efficient synthetic methods.[14]

Among various quinoxaline derivatives, indenoquinoxaline derivatives exhibit a wide range of biological actions, including antimycobacterial,[15] antibacterial, antifungal, antiviral,[16] anticancer,[17] antiprotozoal, and antipasmodial effects.[18–20] Additionally, indeno[1,2-*b*]quinoxalines have been proved as potential acid corrosion inhibitors for mild steel surfaces,[21] utilized in electrical-photochemical materials, dyes, organic semiconductor production, anion receptors, and synthesis of dehydroannulenes, electroluminescent materials and DNA-cleaving agents.[22,23]

Recently, indeno[1,2-*b*]quinoxaline scaffold has garnered considerable attention due to its rigid polycyclic aromatic framework and promising applications in organic electronics, fluorescent probes, and medicinal chemistry.[24] Li and colleagues reported the synthesis of (2,3-bis(4-(dimethylamino)phenyl)quinoxalin-6-yl)(phenyl) methanone by the reaction of 3,4-diaminobenzophenone with benzil using acetic acid under the reflux conditions.[25] Sajjadifar et al., reported the synthesis of 9-methylacenaphtho [1,2-*b*]quinoxaline via one-pot two-component reactions of 3,4-diaminobenzophenone and acenaphthoquinone using phthalic acid as a catalyst at room temperature.[26] Kaya and co-workers reported the synthesis of 7-benzoyl quinoxaline from 3,4-diaminobenzophenone and glyoxal using methanol as a solvent.[27] Mishra and co-workers synthesized 11*H*-indeno[1,2-b]quinoxalin-11-one via ultra-sonication method from *o*-phenylenediamine and ninhydrin using water as a solvent.[28] Kanekar and his groups reported the synthesis of indolo[2,3-*b*]quinoxalin-2-yl(phenyl) methanone from 3,4-diaminobenzophenone and 5-substituted-1-methyl-

[a] *V. Rahimiya, A. Lalitha*
Department of Chemistry, Periyar University, Periyar Palkalainagar, Salem, Tamil Nadu 636011, India
E-mail: lalitha2531@yahoo.co.in

[b] *M. Kalidasan*
Department of Chemistry, Mahendra Arts & Science College, Namakkal, Tamil Nadu 637501, India

[c] *K. B. Sundaram*
Department of Chemistry, PSG College of Arts and Science, Coimbatore, Tamil Nadu 641014, India

1*H*-indole-2,3-dione using acetic acid under the reflux conditions.[29] Different indenoquinoxaline compounds synthesized by methodologies employing catalysts such as MnO_2, $RuCl_2(PPh_3)_3$, OMS-2, $Ga(ClO_4)_3$, and L-proline are reported in the literature.[30,31] Nanocatalysts such cerium oxide, Cu-doped CdS, ZnO, U-alumina, ZMS-5 crystalline SZ, and Ni nanoparticles are also used in the synthesis of quinoxalines.[32–34]

Likewise, our research group has reported earlier the synthesis of several benzoyl-substituted quinoxalines using a condensation strategy involving 1,2-diamines and indan-1,3-dione derivatives. While this earlier work established a convenient route to the core structure, it offered limited exploration of substituent variation and structure-property relationships.[35–37] Compared to all these approaches, our present method offers a more straightforward one-pot strategy under milder conditions, enabling rapid diversification with high yields (up to 92%).

In the present work, the synthesis of 8-benzoyl-11*H*-indeno[1,2-*b*]quinoxaline-11-one derivatives in ethanol through a one-pot two component reaction of 3, 4-diaminobenzophenone (DABP) with different 1,2-dicarbonyl compounds (ninhydrin, isatin, benzil, 2-hydroxynapthoquinone, alloxan or oxalic acid) leading to novel 8-benzoyl-11*H*-ideno[1,2-*b*]quinoxaline-11-one derivatives under greener conditions has been described. From the literature review, it is evident that most of the published researches in this area have limitations such as extended reaction times, complex purification processes, use of many hazardous solvents such as THF, methanol and catalysts such ethylene glycol, acetic acid and H_2SO_4, and low yields. The present work aimed to improve the yields (98%), under catalyst free and greener solvent conditions which lead to eco-friendlier reactions. The present benzoyl analogues show similar/better antimicrobial activity with added ADME profiling and these derivatives show higher GI absorption and broader inhibition spectrum. This study contributes a novel series of benzoyl indenoquinoxaline derivatives that exhibit a substitution-dependent antimicrobial profile with favorable ADME characteristics. The inclusion of comprehensive SwissADME analysis, BOILED-Egg modeling, and structure-activity relationship exploration marks a significant advancement beyond prior quinoxaline studies, many of which lack pharmacokinetic insights or *N*-benzoyl structural diversity.[38]

Spectroscopic analyses were used to characterize the synthesized substances. Additionally, single-crystal X-ray diffraction examinations were used to confirm the molecular structures of two chosen compounds. Computational chemistry tools like DFT methods are successfully used in the mechanistic investigation, to help the complete characterization of the synthesized molecules and also to investigate the molecular orbital interactions.[39–44] The DFT methods helped to study the molecular structure and reactivity descriptors of the benzoyl indenoquinoxaline compounds through electronic structural analysis. In addition, the molecular properties of the optimized structure were defined by computational studies. Molecular docking studies of these compounds showed dynamic binding with human epidermal growth factor receptor tyrosine kinase (4HJO). The newly developed compounds were compared with the traditional antibiotic, *streptomycin*. The in vitro antibacterial activity studies of the synthesized compounds against highly pathogenic bacteria like *S. aureus*, *K. pneumoniae*, and *E. coli* under similar conditions revealed that the benzoyl indenoquinoxaline may be considered as an excellent starting molecule for the synthesis of new bioactive compounds.

2. Experimental Section

2.1. Physical Methods and Materials

All reagents were purchased from commercial sources and used as received. Ninhydrin, alloxan, oxalic acid, benzil, and acenaphthoquinone were acquired through Sigma-Aldrich (Bengaluru, India), 3,4-diaminobenzophenone, isatin derivatives were purchased from Loba Chemie (Hyderabad, India) and used without further purification. The solvents were dried and purified according to standard procedures.[45] All the reactions were carried out at ambient temperature. TLC analysis of all reactions was performed on Merck precoated plates (silica gel 60F-254), and analysed by either placing it in an iodine chamber or under intense UV illumination. Melting points were determined using an Electrothermal 9200 device with the capillary tube method and are uncorrected. IR spectra were recorded on Perkin Elmer FT-IR spectrometer with scanning between 400 and 4000 cm^{-1}. NMR spectra were obtained on Bruker DRX-400 MHz NMR instrument in DMSO-D_6 solvent with TMS as an internal standard. High resolution Mass spectra of representative compounds were recorded with maXis 10138 mass spectrometer operating at 70 eV.

2.2. General Procedure of Synthesis of Quinoxaline Derivatives

Benzoyl indenoquinoxaline derivatives were synthesized by simple cyclocondensation between 3,4-diaminobenzophenone and 1,2-diketone moieties. Equimolar solutions of 3,4-diaminobenzophenone (1) with 1,2 diketones such as ninhydrin (2a), isatin (2b), 5-nitro-isatin (2c), 5-chloroisatin (2d), acenaphoquinone (2e), benzil (2f), 2-hydroxynapthoquinone (2g), alloxan (2h), or oxalic acid (2i) in 10 mL ethanol were stirred without catalyst at room temperature to obtain the corresponding benzoylindenoquinoxaline compounds (3a–i). The progress of the reaction was monitored by TLC (ethylacetate: *n*-hexane, 7:3). Then the precipitate was filtered and washed with water and ethanol in order to obtain the pure product. A single-crystal X-ray study was obtained by recrystallization of these crystals in ethyl acetate/THF mixture.

2.3. X-ray Structure Analyses

Fluorescent orange crystal (3a) and brown crystal (3f) were obtained by the slow evaporation method of THF /Ethyl acetate solutions of the corresponding compounds. Single-crystal X-ray diffraction measurements were carried out on a Bruker D8 Quest Eco diffractometer. Crystal data were collected at 296 K using graphite-monochromatic Mo Kα radiation ($\lambda\alpha$ = 0.7107 Å). The plan for the data collection was calculated using the structure that was solved and refined using the Bruker SHELXTL Software Package. The structures were solved by direct methods using SHELXS-2018/2 and refined by full-matrix least squares with SHELXL-2018/2 refining on F^2.[46,47] Direct methods were used to determine the positions of every atom. All non-hydrogen atoms underwent anisotropic refinement. With isotopic temperature factors that are typically 1.2Ueq of their parent atoms, the hydrogen atoms were arranged in geometrically restricted places.

2.4. Computational Details

2.4.1. Theory

Molecular properties such as chemical hardness (η), electronegativity (χ), electrophilicity (ω), ionization potential (A), and electron affinity (I) have been defined based on the DFT method.[48–51] The chemical reactivity of a molecule can be studied by using chemical hardness. The stability of a molecule is related to its chemical hardness.[52] The ability of an atom within a molecule to draw electrons onto it is known as electronegativity. Chemical hardness (η) and electronegativity (χ) are defined as follows:[53]

$$\text{Chemical Hardness } (\eta) = \frac{1}{2}\left[\frac{\partial^2 E}{\partial N^2}\right]_{V(r)}$$

$$\text{Electronegativity } (\chi) = \frac{1}{2}\left[\frac{\partial E}{\partial N}\right]_{V(r)}$$

where E and V(r) are electronic energy and external potential of an N-electron system, respectively. Using Koopman's theorem for closed shell molecules, η and χ can be defined as follows:

$$I = -\varepsilon_{HOMO},\ A = -\varepsilon_{LUMO}$$

$$\eta = \frac{I - A}{2}$$

$$\chi = \frac{I + A}{2}$$

where I and A are the ionization potential and electron affinity of the molecules, respectively. Ionization potential characterizes the susceptibility of a molecule whereas electron affinity refers to the capability of a ligand to accept precisely one electron from a donor. Electrophilicity (ω) has been proposed as a measure of lowering of energy due to the maximal electron flow between the donor and the acceptor.[54] It can be defined as:

$$\omega = \frac{\chi^2}{2\eta}$$

The $E_{LUMO–HOMO}$ energy gap also included in this study as a quantum mechanical descriptor. There are numerous applications of the HOMO–LUMO energy gap in establishing a correlation between the chemical structure and biological activity.[55–57]

2.4.2. DFT Studies

The DFT calculations were performed with the ORAC software developed by Frank Neese and co-workers.[58] All calculations were carried out using BP86 density functional[59–61] and Def2-TZVP basis set included in the ORCA program, which is free for academic use. The TIGHTSCF convergence criteria has been used while performing the self-consistent field (SCF) calculations. The DFT-optimized geometries were confirmed as minima in the potential energy surface. Pictures of the optimized geometries and the frontier molecular orbitals are taken using the graphics program ChemCraft.[62]

2.5. Molecular Docking Studies

For the docking analysis, BIQ was chosen and subjected to optimization and minimization using LigPrep with the OPLS3 force field. The crystal structure of EGFR tyrosine kinase with (PDB ID: 4HJO) was obtained from the Protein Data Bank.[55] During the preparation process, formal bond orders were assigned, and water molecules were removed. Hydrogen atoms, charges, and any missing side chains of the residues were added to complete the protein structure. The prepared structures were then optimized and minimized to resolve any steric clashes, utilizing the OPLS3 force field and the protein preparation wizard in Schrödinger's Maestro 8.0 software. Following the standard protocol, a grid box was centered on the binding site, identified through site map analysis.[63] The ligands were then docked using the Glide module, which performs flexible ligand docking to find the best fit within the binding site. The resultant protein–ligand complex structure was determined using Biovia discovery studio.[64]

2.6. ADME Analyses

Using the free web server Swiss ADME online tool (http://swissadme.ch/index.php), the bioavailability score, synthetic accessibility, and several pharmacokinetic parameters for the benzoyl indenoquinoxaline derivatives (3h–3i) were analyzed and the most active and positive control were determined.[65,66] Accordingly, for all the synthesized compounds, the calculations were performed using Swiss ADME software, and the results are shown in Tables 11–13.

2.7. Antibacterial Study

Clinically isolated bacterial pathogens of uncultured *Klebsiella* sp. clone MASC-TSK (NCBI-Accession: KF649832.1), *Staphylococcus* sp. MG87 (2013) (NCBI-Accession: KC688883.1). Standard strains of *E. coli* (MTCC-443) were procured from MTCC Chandigarh, India. According to the protocol described in the literature, the newly synthesized benzoyl indenoquinoxaline derivatives 3(a–i) were dissolved in dimethylsulfoxide (DMSO) at a concentration of 25 µg mL^{-1} and tested using the agar well diffusion method against human pathogenic bacteria of Gram negative strain viz., i) *E. coli* (MTCC 443), ii) *K. pneumoniae* (MTCC 424), and Gram positive strain iii) *S. aureus* (MTCC 96).[67,68] The three bacteria exponentially developing cultures in nutrient broth at 37 °C were diluted in sterile broth after 18 h The agar diffusion technique was employed to ascertain the initial screening of antibacterial efficacy. The average diameter of the bacterial growth inhibition zone (IZ) surrounding the disc was measured for each tested drug and disc in mm (Table 14). The standard drug streptomycin was used as a positive control and the bare DMSO solvent was used as negative control. All the samples were taken in triplicates.

2.8. Spectral Details for Synthesis of Benzoyl Indenoquinoxaline Derivatives

2.8.1. 8-Benzoyl-11H-indeno[1,2-b]quinoxaline-11-one (3a)

Yield: 99%; color: yellow solid; M.P: 289 °C; FT-IR (KBr): 3063(CH Str), 1726 (C═O Str), 1654 (C═N Str), 1576, 1487, 1335, 1191, 766, 719 cm^{-1}; ^{1}H NMR (400 MHz, DMSO-D_6): δ 8.54 (d, 1H CH), 8.28 (dd, 1H CH), 8.17 (d, 1H CH), 8.09 (d, 1H CH), 7.89 (m, 3H CH), 7.78 (t, 1H CH), 7.64 (m, 2H CH), 7.53 (t, 2H CH); ^{13}C NMR (400 MHz, DMSO-D_6) δ 194.87, 189.09, 157.97, 150.20, 144.97, 141.63, 141.05, 138.34, 137.04, 136.88, 136.68, 136.69, 134.26, 133.17, 133.06, 132.36, 128.58, 124.88, 122.94; MALDI-TOF: m/z calcd for $C_{22}H_{12}N_2O_2$ 336.08 (M^+), found 338.07.

2.8.2. 9-Benzoylbenzo[4,5]imidazo[1,2-c]quinazolin-6(5H)-one (3b)

Yield: 67%; color: orange solid; M.P:293 °C; FT-IR (KBr): 3384 (NH Str), 2922, 2851, 1649 (C═O Str), 1609 (C═N Str), 1564, 1361, 1214, 1118, 872,

716cm^{-1}; ^{1}H NMR (400 MHz, DMSO-D$_6$): δ 12.53 (s, 1NH), 8.23 (dd, 1H CH), 7.95 (d, 1H CH), 7.79 (dd, 2H CH), 7.72 (m, 2H CH), 7.63 (m, 3H CH), 7.17 (m, 1H CH), 6.83 (dd, 1H CH), 6.59 (m, 1H CH); ^{13}C NMR (400 MHz, DMSO-D$_6$) δ 195.37, 158.28, 155.16, 149.80, 137.37, 137.23, 134.19, 133.35, 132.13, 131.88, 131.65, 130.13, 129.12, 128.50, 124.50, 117.12, 116.82, 114.92; MALDI-TOF: m/z calcd for $C_{21}H_{13}N_3O_2$ 339.10 (M^+), found 340.18.

2.8.3. 9-Benzoyl-2-nitrobenzo[4,5]imidazo[1,2-c]quinazolin-6(5H)-one (3c)

Yield: 75%; color: yellow solid; M.P: 301 °C; yellow solid; FT-IR (KBr): 3345 (NH Str), 2918, 1668 (C═O Str), 1644 (C═N Str), 1593, 1575, 1281, 581cm^{-1}; ^{1}H NMR (400 MHz, DMSO-D$_6$): δ 12.73 (s, 1H NH), 8.70 (d, 2H CH), 8.53 (d 2H CH), 8.05 (dd 2H CH), 7.58 (dd, 2H CH), 7.30 (d, 3H CH); ^{13}C NMR (400 MHz, DMSO) δ 195.62, 195.39, 172.48, 149.67, 147.27, 146.94, 143.18, 140.51, 138.15, 137.68, 136.77, 134.32, 133.13, 132.70, 131.90, 130.13, 129.83, 128.87, 119.55, 114.27, 113.27, 21.52(AcOH); MALDI-TOF: m/z calcd for $C_{21}H_{12}N_4O_3$ 384.08 (M^+), found 386.11.

2.8.4. (8-Chloro-6H-indolo[2,3-b]quinoxalin-3-yl)(phenyl) Methanone (3d)

Yield: 74%; color: yellow solid; M.P: 313 °C; FT-IR (KBr): 3179 (NH Str), 2922, 2851, 1718 (C═O Str), 1629 (C═N Str), 1586, 1466, 1319, 1266, 1185, 706 cm^{-1}; ^{1}H NMR (400 MHz, DMSO-D$_6$): δ 10.71 (s, 1H NH), 7.71 (s, 2H CH), 7.56 (m, 1H CH), 7.43 (m, 1H CH), 7.37 (d, 2H CH), 7.25 (m, 2H CH), 6.97 (m, 1H CH), 6.90 (d, 1H CH); ^{13}C NMR (400 MHz, DMSO-D$_6$): δ 195.20, 155.47, 154.93, 148.00, 147.92, 143.05, 141.69, 137.51, 137.32, 135.30, 134.83, 133.59, 132.84, 131.73, 130.05, 129.11, 127.04, 124.41, 118.49, 117.17, 114.42; MALDI-TOF: m/z calcd for $C_{21}H_{12}$ ClN$_3$O 357.06 (M^+), found 360.14.

2.8.5. Acenaphtho[1,2-b]quinoxalin-9-yl(phenyl) Methanone (3e)

Yield: 83%; color: primrose yellow solid; M.P: 246 °C; FT-IR (KBr): 3042, 1658 (C═O Str), 1633, 1597 (C═N Str), 122, 896, 710 cm^{-1}; ^{1}H NMR (400 MHz, DMSO-D$_6$): δ 8.31 (m, 6H Ar—H), 7.91 (dd, 1H CH), 7.71 (m, 4H Ar—H), 7.57 (m, 4H Ar—H); ^{13}C NMR (400 MHz, DMSO-D$_6$): δ 196.01, 153.26, 138.53, 135.66, 132.55, 131.64, 129.92, 129.65, 128.90, 128.87, 124.87 MALDI-TOF: m/z calcd. for $C_{25}H_{14}$ N$_2$O 358.11 (M^+), found 360.14.

2.8.6. (2,3-Diphenylquinoxalin-6-yl)(phenyl) Methanone (3f)

Yield: 83%; color: crystalline brown solid; M.P: 294 °C; FT-IR (KBr): 3054, 1659 (C═O Str), 1596 (C═N Str), 1444, 1346, 1267, 816, 691cm^{-1}; ^{1}H NMR (400 MHz, DMSO-D$_6$) δ 8.36(d, 1H CH), 8.31 (d, 1H CH), 8.20 (dd, 1H CH), 7.87(d, 2H CH), 7.75 (m, 1H CH), 7.63 (m, 3H CH), 7.51 (m, 4H Ar—H), 7.39 (m, 6H Ar—H); ^{13}C NMR (400 MHz, DMSO) δ 195.38, 155.23, 154.67, 142.57, 139.89, 138.80, 138.78, 138.34, 137.08, 133.55, 131.82, 130.27, 130.22, 130.13, 130.06, 129.95, 129.87, 129.66, 129.52, 129.17, 128.57, 128.55; MALDI-TOF: m/z calcd for $C_{27}H_{18}N_2O$ 386.14 (M^+), found 388.17.

2.8.7. (5-Hydroxybenzo[a]phenazin-9-yl)(phenyl) Methanone (3g)

Yield: 59%; color: orange solid; M.P: 289 °C; FT-IR (KBr): 3042, 1658 (C═O Str), 1633, 1597 (C═N Str), 1536, 1480, 1322, 1142, 710 cm^{-1}; ^{1}H NMR (400 MHz, DMSO-D$_6$): δ 11.71 (s, 1 OH), 9.30 (s, 1H CH), 8.35 (dd, 3H Ar—H), 8.16 (d, 1H CH), 7.93 (m, 4H Ar—H), 7.76 (t, 1H CH), 7.65 (d, 2H CH), 7.20 (s, 1H CH). ^{13}C NMR (400 MHz, DMSO-D$_6$): δ 194.13, 161.60 (C-OH), 143.61, 139.37, 131.65, 129.31, 128.67, 127.32, 126.64, 125.51, 120.48, 114.05; MALDI-TOF: m/z calcd for $C_{23}H_{14}$ N$_2$O$_2$ 350.10 (M^+), found 352.02.

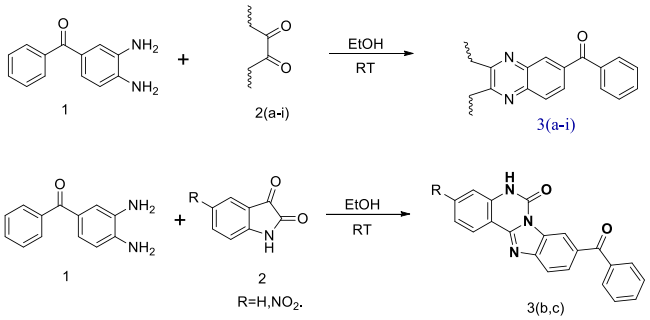

Scheme 1. Synthesis of quinazolinone-fused quinoxaline derivatives.

2.8.8. 7-Benzoylbenzo[g]pteridine-2,4(1H,3H)-dione (3h)

Yield: 89%; color: yellow solid. M.P: 292 °C; FT-IR (KBr): 3349, 1660 (C═O Str), 1646 (C═N Str), 1597, 1487, 1283, 704 cm^{-1}; ^{1}H NMR (400 MHz, DMSO-D$_6$): δ 11.32, 9.82 (s, 2NH), 8.26 (s 1H CH), 8.12 (s, 1H CH), 7.63 (d, 1H CH), 7.42 (d, 1H CH), 7.19 (m, 4H Ar—H); ^{13}C NMR (400 MHz, DMSO-D$_6$): δ 195.92, 152.56, 140.39, 138.03, 137.16, 136.84, 132.93, 132.72, 130.00, 129.91, 129.36, 129.00, 126.66, 125.83, 117.97, 115.22; MALDI-TOF: m/z calcd for $C_{17}H_{16}$ N$_4$O$_3$ 318.07 (M^+), found 318.08.

2.8.9. 6-Benzoylquinoxaline-2,3(1H,4H)-dione (3i)

Yield: 89%; color: yellow solid. M.P: 3177 °C; FT-IR (KBr): 3354, 2607, 1655 (C═O Str), 1623 (C═N Str), 1571, 1517, 1454, 1331, 1295, 759 cm^{-1}; ^{1}H NMR (400 MHz, DMSO-D$_6$): δ 7.63 (s, 1H), 7.60 (d, 2H), 7.56 (d, 1H), 7.51 (d, 3H), 7.03 (d, 2H), 6.64 (d, 2H NH); ^{13}C NMR (400 MHz, DMSO-D$_6$): δ 194.47, 162.48, 142.30, 139.77, 132.25, 131.40, 129.29, 128.56, 125.66, 124.28, 117.36, 113.14; MALDI-TOF: m/z calcd for $C_{15}H_{10}N_2O_3$ 266.09 (M^+), found 266.07.

3. Results and Discussion

3.1. Synthesis of Benzoyl Indenoquinoxaline and Optimization of Reaction Conditions

The synthesis of novel 8-benzoyl-11*H*indeno[1,2-*b*]quinoxaline-11-one (3a) has been achieved by the cyclocondensation process of 3,4-diaminobenzophenone (1) (1.0 mmol) with ninhydrin (2a) (1.0 mmol) as model substrates under neat conditions at room temperature. The product was separated in good yields and purified by recrystallization. Similar procedures were also followed for the synthesis of other derivatives. All these compounds are yellow–orange crystalline solids, resulting as air-stable and non-hygroscopic products. They are soluble in THF, DCM, acetonitrile, acetone, toluene, 1,4-dioxane, and DMSO and sparingly soluble in chloroform and methanol.

The reaction of 2-fold excess of isatin with 3,4-diaminobenzophenone afforded compound imidazo[1,2-*c*]quinazoline as a sole product. An unexpected five-membered heterocyclic compound was formed when an electron-withdrawing substituent is present in isatin, such as nitroisatin in the formation of imidazoquinazoline (Scheme 1). All the synthesized compounds were analyzed by analytical techniques such as ^{1}H NMR, ^{13}C NMR, IR, and electronic spectroscopy, as

Table 1. Optimization of an appropriate solvent.[a)]

S. No.	Solvent	Temp (°C)	Time (h)	Yield %[b)]
1	Water	RT	6	15
2	**Ethanol**	**RT**	**3**	**98**
3	Ethanol: Water	RT	4	43
4	Methanol	RT	3	78
5	Methanol: Water	RT	4.5	37
6	Acetonitrile	RT	8	20
7	PEG	RT	5	21
8	Glycerol	RT	12	–

[a)] Reaction conditions: 3,4-diaminobenzophenone (1.0 mmol) and ninhydrin (1.0 mmol) with different solvents (10.0 mL) at room temperature;
[b)] Isolated yields.

Table 2. Optimization of appropriate temperature (°C).[a)]

S. No	Solvent	Temp (°C)	Time (h)	Yield %[b)]
1	**Ethanol**	**RT**	**3**	**98**
2	Ethanol	40	3	78
3	Ethanol	50	3	72
4	Ethanol	60	3	68
5	Ethanol	65	3	55
6	Ethanol	70	3	40
7	Ethanol	80	3	38
8	Ethanol	Reflux	3	35

[a)] Reaction conditions: 3,4-diaminobenzophenone (1.0 mmol) and ninhydrin (1.0 mmol) with ethanol (10.0 mL) at different temperatures.
[b)] Isolated yields.

well as mass spectrometry. The structure of compounds 3a and 3f was also described by single-crystal XRD methods.

The model one-pot two-component condensation of 3,4-diaminobenzophenone (1) (1.0 mmol) with ninhydrin (2a) (1.0 mmol) was used for various optimization studies. Initially the reaction was performed in solvents of different polarity, such as ethanol, methanol, PEG-300, ethylene glycol, diethyleneglycol, acetonitrile, DMF, and dioxane as shown in the Table 1. The resulting yield was found to be 98% in ethanol after 3 h (Table 1, Entry 2), when compared to the other solvents, where the yields were moderate (20%–78%) at room temperature.

The effect of temperature on the reaction time and the yields of products show that the reaction was strongly influenced by the temperature. Consequently, we have made efforts to increase the percentage of yield by optimizing the temperature suitable for the reaction by changing the conditions from room temperature to reflux conditions. It was observed that the room temperature conditions afforded a better yield of 98% with a reaction time of 3 h in ethanol (Table 2, Entry 1). Increase in temperature by 10 °C up to 80 °C did not show any increase in the product yield and on contrary the yield decreases with increase in the temperature.

Next, the model reaction was screened with different catalysts like piperidine, 2-aminopyridine, H_2SO_4, triethylamine and NaOH in order to reduce the reaction time. The reaction in the case of ethanol with piperidine as a catalyst did not yield any product even after 24 h. It is evident that, with catalyst, the yield of the product was decreased (Table 3, Entry 2–6). From the above optimization studies, it was evident that the suitable condition for the formation of a good yield of product was the room temperature in ethanol without any catalyst. Further derivatives were prepared under these optimized conditions as shown in the Table 4.

A proposed mechanism for the reaction is described in Scheme 2. At first, 3,4-diaminobenzophenone reacts with isatin to give the intermediate (A) by deprotonation of amino group. The other amino group undergoes intramolecular cyclization to isatin (B) with the elimination of water molecule forming the intermediate (B). C—C bond cleavage occurs to give intermediate (C) in which the intramolecular the attack of amino group to ketone occurs to provide the corresponding product.

4. X-ray Crystallographic Studies

Molecular structure of benzyl indenoquinoxaline compounds (3a) and (3f) were confirmed by single-crystal XRD method.

Table 3. Optimization of appropriate catalyst.[a)]

S. No.	Catalyst	mol%	Solvent	Temp (°C)	Time (h)	Yield %[b)]
1	**Without catalyst**	–	**Ethanol**	**RT**	**3**	**98**
2	Pyridine	10	Ethanol	RT	6	–
3	Acetic acid	10	Ethanol	RT	3	75
4	H_2SO_4	5	Ethanol	RT	4	80
5	Dioxane	10	Ethanol	RT	24	63
6	Piperidine	10	Ethanol	RT	4.5	–
7	L-Proline	10	Ethanol	RT	12	10
8	Et_3N	10	Ethanol	RT	8	–
9	NaOH	10	Ethanol	RT	24	–

[a)] Reaction conditions: 3,4-diaminobenzophenone (1.0 mmol) and ninhydrin (1.0 mmol) with different catalysts in ethanol (10.0 mL) at room temperature.
[b)] Isolated yields.

Research Article
doi.org/10.1002/slct.202502878

Chemistry Europe
European Chemical Societies Publishing

Table 4. Synthesis of novel quinazolinone-fused quinoxaline derivatives (3a–i) using ethanol under catalyst-free condition.[a)]

S. No	Diketone	Product	Time (h)	m.p. (°C)	Yield %[b)]
1	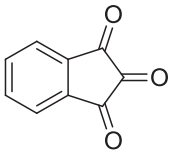	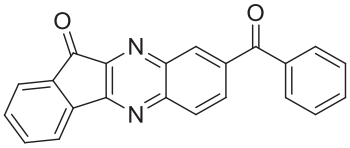	3	289	98
2	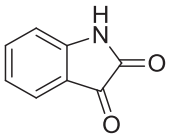	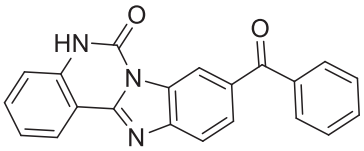	3.5	293	63
3	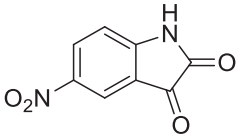	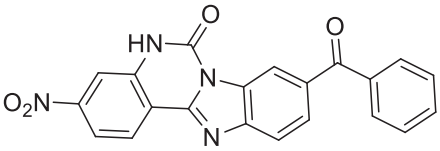	3	301	87
4	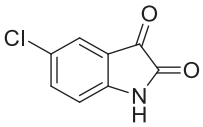	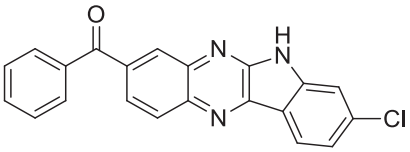	2.5	304	76
5	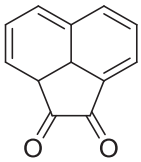	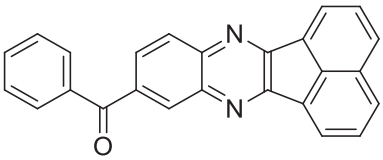	3.5	246	82
6	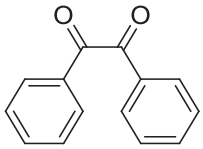	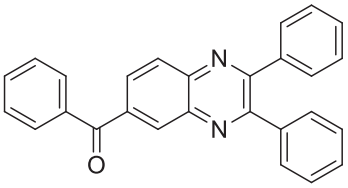	8	294	93
7	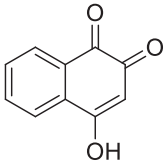	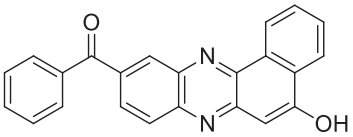	1.5	289	98
8	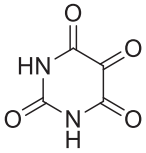	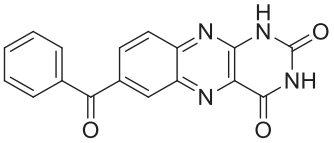	4	294	93
9	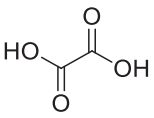	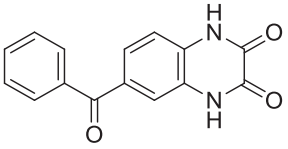	5.5	317	60

[a)] Reaction conditions: 3,4-diaminobenzophenone (1.0 mmol) and diketone (1.0 mmol) in ethanol (10.0 mL) at room temperature.
[b)] Isolated yields.

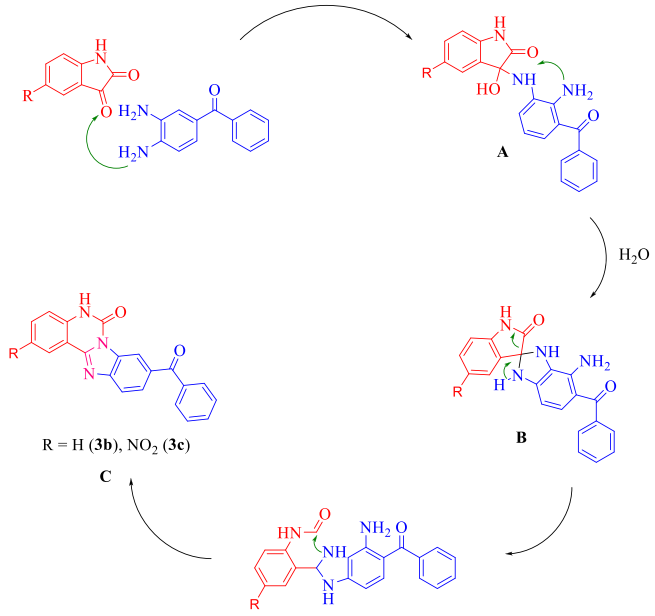

Scheme 2. Proposed mechanism for the formation of 9-benzoylbenzo[4,5]imidazo[1,2-*c*]quinazolin-6(5*H*)-one.

The suitable crystals for X-ray crystallographic analysis were obtained by slow evaporation of benzyl indenoquinoxaline compound in ethyl acetate/THF. Crystallographic details are summarized in Table 5. The selected bond lengths and angles are presented in Tables 6 and 7. Molecular structure of compounds 3a and 3f were drawn with ORTEP-3 and showed in Figures 1 and 2. Compounds 3a and 3f are crystallized in the monoclinic with the space group P1 21/n1. The X-ray structure analysis of compounds 3a and 3f have showed that, 3,4-diaminobenzophenone condense with ninhydrin or benzil to form quinoxaline compounds as confirmed by bond lengths of C=N 1.2989 & 1.3092 (3a) and 1.364 and 1.366 (3f) and are in good agreement with those of similar compounds reported earlier. Non-substituted indeno[1,2-*b*]quinoxaline exhibits planar geometry with extended π-conjugation. Our compound displays slight distortion in planarity due to the benzyl group's steric bulk, which can be observed in the single-crystal X-ray data.[25]

From the ORTEP view of the compound 3a, it is evident that the compound is nearly planar in nature (anti-periplanar conformation) due to the torsion angle between the mean plane of the quinoxaline ring (C8/C9) and benzoyl ring (C9/C10/O2) is -152.1(1)°, −141.7(1)°, and −134.8(1)° for the atoms C8—C9—C10—C19, C8—C9—C10—C18 and C7—C8—C9—O2, respectively. Moreover, intramolecular hydrogen bonds of the type C···O stacking were observed in compound 3a between the quinoxaline moiety (C6) and oxygen atom of (O2) benzoyl moiety at bond length of 3.126 A° as shown in Figure 3.

The molecular structure of compound 3f, reveals that the phenyl rings are located at the 2,3-position of the quinoxa-

Table 5. Crystallographic and structure refinement parameters for compounds 3a and 3f.

Compound	3a	3f
Chemical formula	$C_{22}H_{12}N_2O_2$	$C_{27}H_{18}N_2O$
Formula mass	336.08	386.43 g/mol
Crystal system	Monoclinic	Monoclinic
Crystal habit	Fluorescent orange	Fluorescent light brown block
a/Å	11.8318(4) Å	14.8221(9) Å
b/Å	10.1634(5) Å	6.1537(3) Å
c/Å	14.1195(7) Å	22.9513(15) Å
α/°	90°	90°
β/°	107.443(2)°	107.223(3)°
γ/°	90°	90°
Unit cell volume/Å3	1619.81(13) Å3	1999.5(2) Å3
Temperature/K	296(2) K	296(2) K
Space group	P1 21/n 1	P1 21/n 1
Z	4	4
Index ranges	$-15 \le h \le 15$, $-13 \le k \le 13$, $-18 \le l \le 18$	$-18 \le h \le 19$, $-7 \le k \le 8$, $-28 \le l \le 28$
Reflection collected	49187	13364
Independent reflections	4036 [R(int) = 0.0301]	4668 [R(int) = 0.0710]
Data/ restraints/ parameters	4036/0/235	4668/0/271
Goodness-of-fit on F^2	1.050	1.000
Final R indices	3291 data; $I > 2\sigma(I)$ R1 = 0.0656, wR2 = 0.2146 all data R1 = 0.0762, wR2 = 0.2298	2588 data; $I > 2\sigma(I)$ R1 = 0.0632, wR2 = 0.1531 all data R1 = 0.1288, wR2 = 0.1933
Largest diff. peak and hole	0.300 and −0.540 eÅ-3	0.184 and −0.225 eÅ-3

Table 6. The selected bond length and bond angle of compound 3a.

Atoms	Bond Length		Atoms	Bond Angle	
	XRD	DFT		XRD	DFT
N1—C8	1.2989 (15)	1.310	C8—N1—C15	114.1 (10)	114.4
N1—C15	1.3784 (14)	1.374	N1—C15—C14	118.4 (10)	118.7
N2—C9	1.3092 (15)	1.317	N1—C15—C10	121.7 (11)	121.8
N2—C10	1.3787 (16)	1.374	C9—N2—C10	114.2 (10)	114.4
O1—C7	1.2052 (12)	1.218	N2—C9—C8	123. 1(11)	123.5
C15—C14	1.4057 (17)	1.414	N2—C10—C11	119.3 (11)	119.3
C18—C19	1.3810 (3)	1.392	N2—C10—C15	122.2 (10)	121.1
C13—C12	1.4120 (2)	1.423	O1—C7—C5	128.2 (12)	127.8
C4—C3	1.3807(19)	1.394	N1—C8—C9	124.5 (10)	123.9
C21—H11	1.0200 (2)	1.09	O1—C7—C8	127.6(12)	127.8
C16—O2	1.2223(18)	1.231	N1—C8—C7	127.3(10)	127.6
C12—H6	0.9690(17)	1.09	O2—C16—C17	121.7(14)	120.6
C22—H12	1.021(18)	1.09	O2—C16—C13	118.7(14)	119.1

Table 7. The selected bond length and bond angle of compound 3f.

Atoms	Bond Length		Atoms	Bond Angle	
	Exp.	DFT		Exp.	DFT
N1—C5	1.364 (3)	1.359	C5—N1—C6	117.4 (2)	118.65
N1—C6	1.327 (3)	1.327	C12—N2—C6	117.2 (2)	118.71
N2—C17	1.366 (3)	1.361	N1—C4—C6	120.9 (2)	120.39
N2—C16	1.315 (3)	1.326	N2—C6—C3	118.9 (2)	120.08
O1—C10	1.221 (3)	1.230	N2—C6—C4	121. 2 (2)	120.28
C9—C10	1.493 (3)	1.504	N2—C12—C5	121.8 (2)	120.48
C10—C11	1.490 (3)	1.500	N2—C12—C17	114.9 (2)	115.63
C4—C6	1.407(4)	1.432	O11—C13—C7	119.6 (2)	119.93
C5—C12	1.439 (4)	1.456	N1—C4—C8	120.3 (2)	120.22

line nucleus with the dihedral angles 39.12° and 50.55° while benzoyl ring is located at the 7-position of the quinoxaline moiety with the dihedral angle −47.69°. Additionally, due to steric hindrance, the average twist angle of the phenyl ring at the 2,3-position is significantly greater than the twist angle of the substituent at the 7-position. On the other hand, $\pi-\pi$ interactions were observed between adjacent molecules in the crystal packing with the bond distance 3.373 Å and also were connected via C···O (C6···O1) interaction with bond distance of 3.064 Å. Compound 3f is a mutual chimeric stacking mode because of the high molecular interaction, as seen in Figure 4.

Molecular structure of compounds 3a and 3f were drawn with ORTEP-3 and showed in Figures 1 and 2.

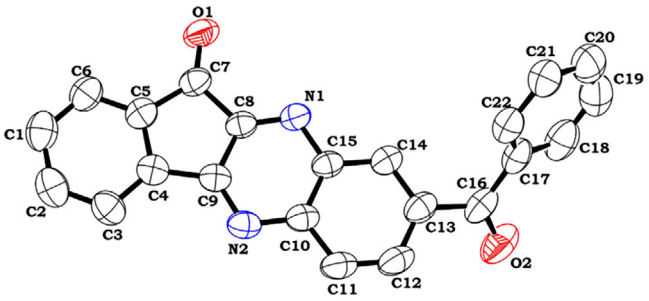

Figure 1. ORTEP diagram of compound 3a.

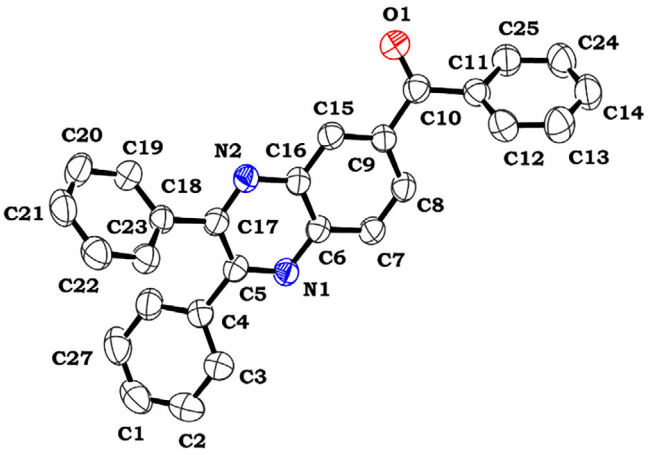

Figure 2. ORTEP diagram of compound 3f.

4.1. DFT Studies

4.1.1. Geometric Optimization

The geometry of the title compounds is optimized by the density functional theory (DFT) method at the BP86/Def2-TZVP level using the program ORCA. The optimized structures of compounds 3a and 3f have been shown in Figures 5 and 6. Theoretical and X-ray data for bond angles and bond distance are given in Tables 6 and 7, respectively. Geometry optimization of the compounds 3a and 3f leads to the minimum energy structure with no imaginary frequencies and confirms that optimized geometries are minimum energy structures in the potential energy surface. The DFT (BP86/Def2-TZVP) computed bond parameters of the compounds 3a and 3f exist in good agreement with those of the experimentally obtained X-ray diffraction data values.

4.1.2. Electronic Properties/Frontier Molecular Orbital Analysis

Using the ORCA software, the electric properties of compounds 3a and 3f are computed at the BP86/Def2-TZVP level of theory. The HOMO and LUMO energy values are used to calculate and evaluate conceptual density functional theory properties such as global softness, electrophilicity index, chemical potential, and global hardness. The reactivity of a molecule is controlled at the molecular level by the frontier molecular orbitals (FMO), viz. HOMO and LUMO. The energy difference between HOMO and

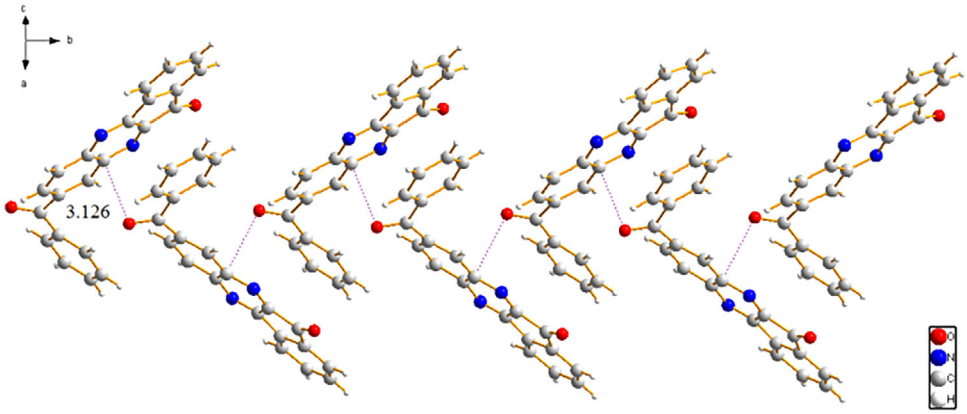

Figure 3. C···O stacking interaction of compound 3a.

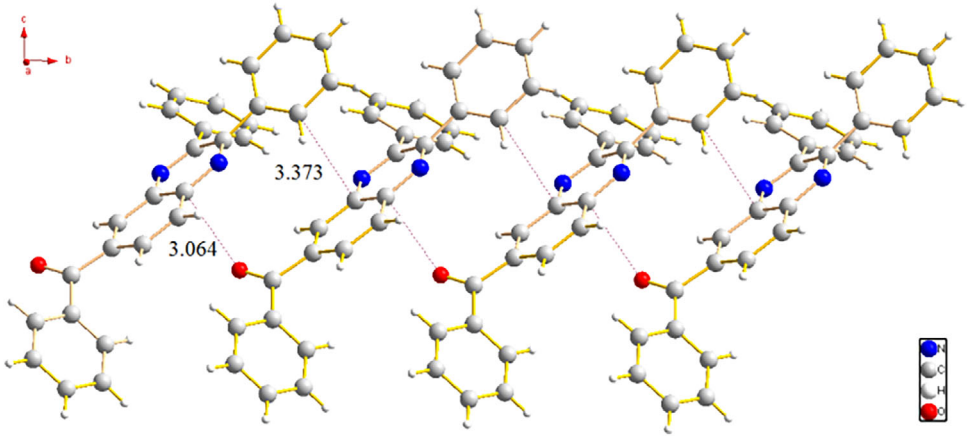

Figure 4. π···π and C···O stacking interaction of compound 3f.

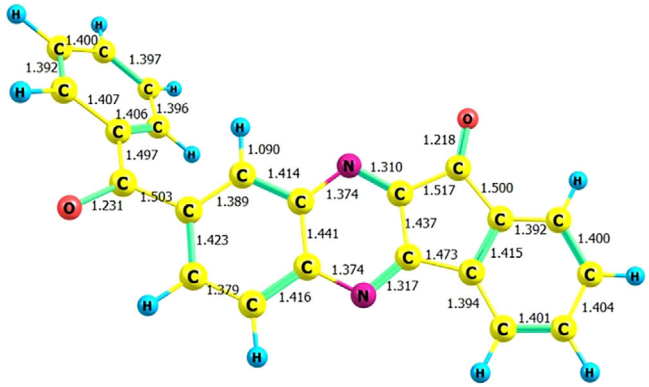

Figure 5. DFT (BP86/Def2-TZVP) optimized geometry of compound 3a.

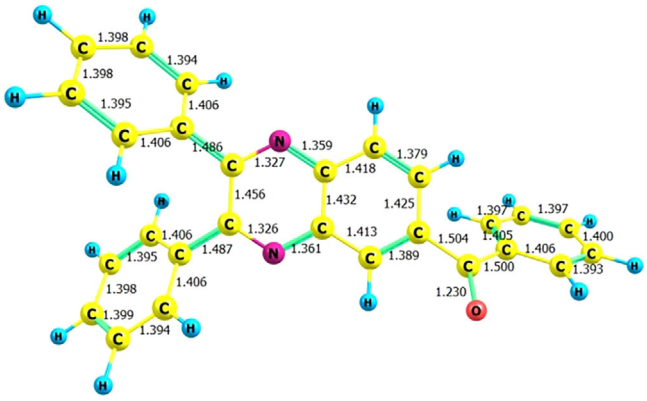

Figure 6. DFT (BP86/Def2-TZVP) optimized geometry of compound 3f.

LUMO gives the energy of band gap which is used to predict the kinetic stability, chemical reactivity of the molecules and to determine electrical and optical properties, which are the most important parameters of quantum chemistry. The highest occupied molecular orbital and lowest unoccupied molecular orbitals of the compounds 3a and 3f in the gas phase are shown in Figure 7. The electronic properties of the compound 3a and 3f were obtained from the calculated HOMO and LUMO energies and listed in Table 8.

The compound 3a and 3f showed $E_{LUMO–HOMO}$ energy gap value of 1.97 and 2.47 eV, respectively, confirming the more stable nature of 3f when compared to 3a. The molecule's ability to donate electrons is shown by the E_{HOMO} value in HOMO–LUMO energy, whereas its ability to accept electrons is indicated by the E_{LUMO} value. Compared to molecules having a high energy gap, those with a smaller energy gap have more chemical reactivity. The electrophilicity index values of 3a and 3f confirm the

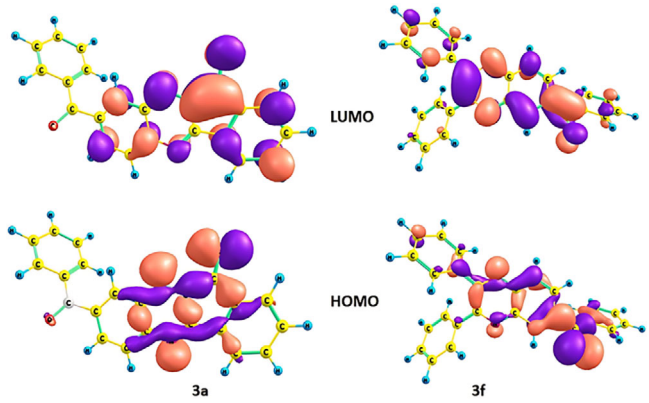

Figure 7. Frontier molecular orbitals of the compounds 3a and 3f.

Table 8. DFT (BP86/Def2-TZVP) computed electronic properties of compounds (3a) and (3f).

Electronic Properties		Values (eV) 3a	3f
Ionization Potential	$I = -E_{HOMO}$	5.8574	5.8240
Electron affinity	$A = -E_{LUMO}$	3.8857	3.3534
Energy gap	$(\Delta E = (E_{LUMO}-E_{HOMO})$	1.9717	2.4706
Electronegativity	$\chi = (I + A)/2$	4.8716	4.5887
Molecular hardness	$\eta = (I - A)/2$	0.9859	1.2353
Molecular softness	$S = 1/\eta$	1.0143	0.8095
Chemical potential	$\mu = -\chi$	−4.8716	−4.5887
Electrophilic index	$\omega = \mu^2/2\eta$	12.0360	8.5227
Dipole moment (Debye)		2.9465	3.0636

more electrophilic nature of the compound 3a (12.04 eV) when compared to that of 3f (8.02 eV).

4.1.3. ^{1}H and ^{13}C NMR Spectral Studies

Computational chemistry tools like DFT methods can also be used to predict the isotropic magnetic shielding of the atoms individually and can assist the ^{1}H and ^{13}C spectral assignments. This method can aid if there is a mixture of isomers or trivial hydrogen atoms, bridging hydrogen atoms etc., Gauze induced atomic orbital (GIAO) method has been used to compute the isotropic magnetic shielding of the compounds 3a and 3f. The isotropic magnetic shielding is then used to calculate the chemical shift values of the individual atoms by considering the tetramethylsilane as reference. The DFT (Def2-TZVP) compute ^{1}H and ^{13}C NMR chemical shift values for compound 3a is given in the Table 9.

Experimentally nineteen ^{13}C NMR signals were obtained for the 22 carbon atoms of the compound 3a. The DFT method was useful to assign the chemical shift values of the 22 carbon atoms individually and the DFT computed values are in close agreement with those of the experimentally by obtained ^{13}C and ^{1}H chemical shift values (Table 9 and Figure 8). In the ^{13}C NMR spectra the two carbonyl carbon atoms resonate at 194.87 and 197.7 ppm, respectively. In the ^{1}H NMR spectra eight signals are obtained for the twelve hydrogen atoms. DFT methods predict the chemical shift values for the individual hydrogen atoms. From DFT computations, among the five hydrogen atoms of the phenyl ring attached to carbonyl group, four resonate around 7.6–7.8 ppm and the remaining hydrogen atom which is spatially close to C═O group resonate at 8.46 ppm.

Table 9. The DFT (Def2-TZVP) computed ^{1}H and ^{13}C NMR chemical shift values for compound 3a. Experimental values are given and DFT computed values are in square brackets.

Atoms	Chemical Shift ppm	Atoms	Chemical Shift ppm
^{13}C NMR		C34	132.36 [132.42]
C5	136.69 [136.0]	C36	144.97 [147.0]
C7	124.88 [126.92]	C37	122.94 [125.69]
C9	141.05 [142.92]	C32	133.17 [134.67]
C10	189.09 [197.7]	C30	138.34 [138.24]
C11	157.97 [155.92]	^{1}H NMR	
C12	144.97 [147.87]	H6	[7.677]
C13	136.88 [139.63]	H8	[7.93]
C15	141.63 [142.87]	H14	[8.573]
C16	194.87 [200.14]	H19	[7.988]
C17	[142.02]	H21	[7.658]
C18	133.06 [134.97]	H23	[7.802]
C20	128.18 [130.33]	H25	[7.808]
C22	134.26 [136.04]	H29	[8.352]
C24	139.69 [139.62]	H31	[8.696]
C26	157.97 [163.4]	H33	[8.462]
C27	150.20 [148.5]	H35	[7.811]
C28	137.04 [135.07]	H38	[8.271]

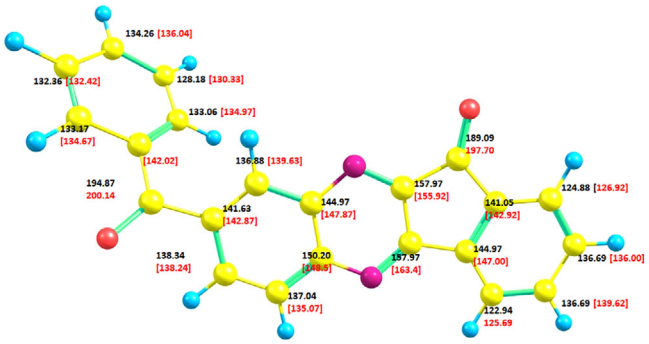

Figure 8. The DFT (Def2-TZVP) computed ^{13}C NMR chemical shift values for compound 3a are provided in the square brackets along with experimental values.

4.2. Molecular Docking

Molecular docking studies demonstrate both ligand-protein interaction and the effectiveness of probe molecules in preventing diseases. To assess the synthetic drugs' binding affinities and inhibitory mechanisms, molecular docking studies were conducted using the chosen protein as the host. Induced-fit docking

Table 10. Intermolecular interacting residues between synthesized benzoyl indeno quinoxaline derivatives (3a–i) with 4HJO.

S. No.	Compound Name	Docking Score	Hydrophobic Interactions	Hydrogen Bonds
1	3a	−6.86	GLUA:179, TRPA:436, CYSA:182, ASPA:246, HISA:270, TRPA:361, HISA:193.	TYRA:134.
2	3b	−8.72	TRPA:436, GLUA:389, CYSA:182, PHEA:452.	GLUA:179, TYRA:134.
3	3c	−8.42	PHEA:321, PHEA:344, TRPA:436, GLUA:389, TRPA:361, HISA:193, LEUA:186.	TYRA:134, TYRA:360.
4	3d	−5.83	TYRA:360, TRPA:361, TRPA:436, TYRA:318, LEUA:186.	ASNA:190.
5	3e	−7.73	TRPA:361, GLUA:389, CYSA:182, TYRA:436, CYSA:182, VALA:248.	TYRA:360, TYRA:134.
6	3f	−8.87	PHEA:452, PHEA:344, TRPA:436, GLUA:389, GLUA:443, TYRA:318 TRPA:340, HISA:270, VALA:248.	TYRA:134.
7	3g	−6.53	VALA:248, HISA:270, ARGA:181.	TYRA:250, TYRA:134.
8	3h	−6.99	GLUA:179, TRPA:361, GLUA:389, HISA:193, CYSA:182, TYRA:436.	TYRA:360, TYRA:134.
9	**3i**	**−9.08**	**GLUA:443, PHEA:452, TYRA:318, TRPA:436, GLUA:179, TYRA:134, TRPA:361, HISA:133, PHEA:321, THRA:319, ASPA:246.**	**GLNA:32, TRPA:444.**

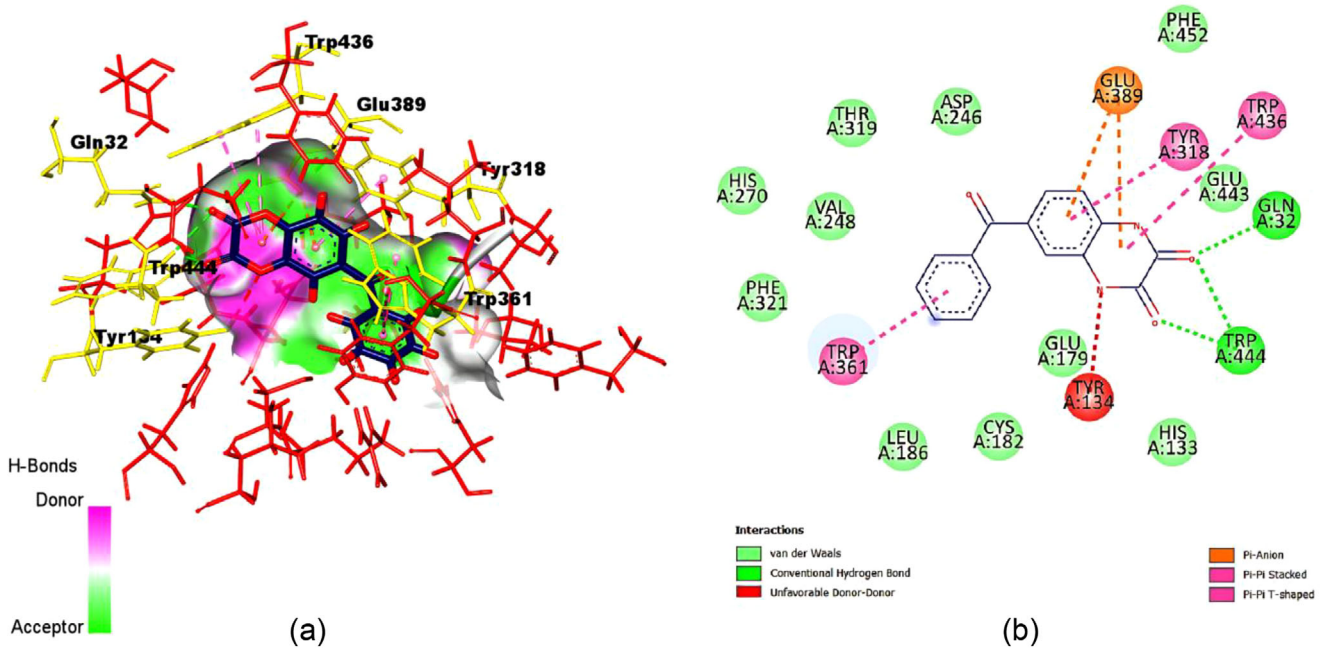

Figure 9. a) 3D structure and b) 2D structure of compound 3i and its interaction with amino acid 4HJO.

is the best method for determining the binding affinity between a ligand and an enzyme because of the flexibility of both throughout the docking process. A number of intermolecular interactions involving amino acid residues were used to determine the synthesized compounds 3(a–i) binding affinity, given in the Table 10. 3D Structure of compound 3i and its interaction with amino acid 4HJO is provided in Figure 9a, whereas the 2D structure of compound 3i showing the ligand interaction with amino acid 4HJO is given in Figure 9b. The quinoxaline ring occupied the hydrophobic pocket II enclosed by frequently LEU residues as van der Waals bonding interaction with: GLUA:443, PHEA:452, GLUA:179, HISA:133, PHEA:321, THRA:319, ASPA:246 and covalent hydrogen bonding interaction with GLNA:32, TRPA:444, and a docking score of −9.08 kcal/mol. Other recent studies on similar indenoquinoxaline scaffolds have reported docking outcomes mainly in the −7.0 to −8.5 kcal/mol range.[69–71] However, these structures typically lack benzoyl substitution or electronic modulation, and often do not report interaction profiles in detail. In contrast, our current results reveal that judicious substitution on the benzoyl group leads to improved binding specificity

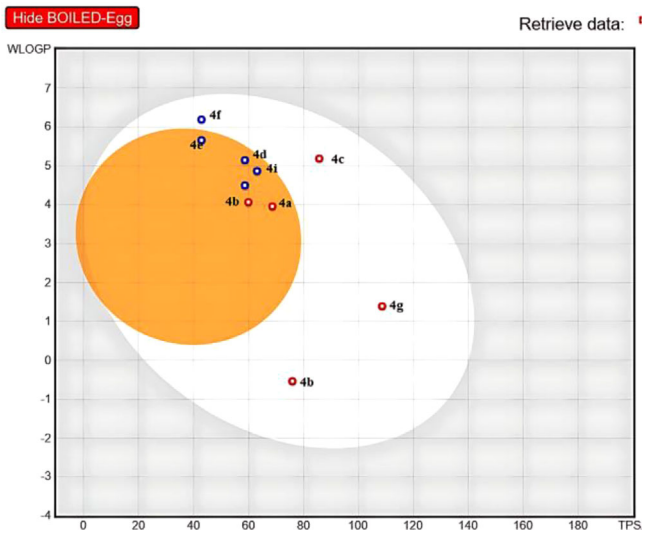

Figure 10. BOILED-Egg plot of benzoyl indenoquinoxaline (3a–i) using SwissADME web tool.

and enhanced pharmacophoric interactions. In summary, the theoretical in silico molecular docking scores provided strong evidence for the bacterial inhibitors. The results of the in vitro antibacterial activity studies were found to be in good arrangement with the theoretical values obtained with the molecular docking. These improvements not only align with green chemistry principles but also demonstrate enhanced sustainability and operational simplicity. Moreover, the synthesis of the title compounds present more advantages compared to our previous similar report[70] in such a way that the reaction is possible under room temperature instead of reflux conditions. The time consumed and the % yield of the products show the superiority of the present protocol. The studied compounds exhibited an enhanced zone of inhibition compounds to our previous work.[70]

4.3. ADME (Absorption, Distribution, Metabolism, and Excretion) Prediction

The ADME calculations were performed for the synthesized compounds (3a–i) for the assessment of drug pharmacokinetic and drug-like qualities using SwissADME web tool. The Lipinski's rule of five predicts the oral bioavailability of a synthesized compound based on its physicochemical properties. According to this rule, a molecule will act as orally active drug if its molecular weight is less than 500 (m/z) and it should not contain more than five hydrogen bond donors and not more than 10 hydrogen bond acceptors. In addition, the lipophilicity (cLogP) should be lesser than 5. If the synthesized molecules exhibit more than one violation of the aforementioned criteria, then the compounds will not be considered as drugs. The bioavailability scores, as well as certain pharmacokinetic properties for the full active and the BOILED-Egg plot of compounds have been provided in Figure 10 and the results are shown in Tables 11–13. The molecular weights of the synthesized compounds lie in the range 320.24–416.15, which is well within the limits. The compounds fascinated to know that the parameters like the number of rotatable bonds and topological polar surface area (TPSA) are important factors of oral bioavailability of pharmaceuticals and highly helpful physicochemical factors for predicting drug transport characteristics.

Moreover, for a drug TPSA should be less than 140 Å2 and its number of rotatable bonds too less than ten as predicted by Veber rule. The formula % Abs = 109 − 0.345 × TPSA[72] was used to determine the percentage of absorption and displaced in Table 11. All the compounds exhibited favorable pharmacokinetic properties, including high gastrointestinal absorption,

Table 11. In silico prediction of physicochemical, drug-likeness properties, and medicinal chemistry parameters for most active quinoxaline derivatives.

S. No.	Compound	RB[a]	MR[b]	Physicochemical Parameters					Lipinski's Violation	% Abs
				TPSA[c] Å^2	MW[d] (<500)	HBA[e] (<10)	HBD[f] (<5)	ilogPo/w[g] (<5)		
1	3a	2	98.28	59.92	336.34	4	0	3.55	0	88.3276
2	3b	2	98.78	58.64	323.35	3	1	3.90	0	88.7692
3	3c	2	103.79	58.64	357.79	3	1	4.44	0	88.7692
4	3d	2	106.45	63.08	350.37	4	1	4.11	0	87.2374
5	3e	2	111.35	48.85	358.39	3	0	4.77	0	92.1468
6	3f	4	120.28	42.85	386.44	3	0	5.23	0	94.2168
7	3g	2	88.16	108.57	318.29	5	2	1.90	0	71.5434
8	3h	2	75.29	75.93	264.24	5	0	1.38	0	82.8042
9	3i	4	129.89	85.70	440.45	6	0	4.55	0	79.4335

[a] Number of rotatable bonds.
[b] Molar refractivity.
[c] Topological polar surface area.
[d] Molecular weight.
[e] Hydrogen bond acceptors.
[f] Hydrogen bond donors.
[g] ilog$P_{o/w}$, in-house physics-based method implemented for the calculation of lipophilicity.

Table 12. In silico prediction of lipophilicity parameters for most active quinoxaline derivatives.

S. No.	Compound	Lipophilicity Properties				
		LogPo/w (iLOGP)	LogPo/w (XLOGP3)	LogPo/w (WLOGP)	LogPo/w (MLOGP)	LogPo/w (SILOCOS-IT)
1	3a	2.46	4.06	4.07	2.16	4.98
2	3b	2.60	4.44	4.50	3.12	4.87
3	3c	2.87	5.06	5.15	3.60	5.50
4	3d	2.83	4.87	4.87	3.11	4.87
5	3e	3.36	5.20	5.66	3.54	6.07
6	3f	3.73	5.87	6.19	3.91	6.43
7	3g	1.35	1.74	1.39	1.52	3.50
8	3h	1.17	1.31	−0.54	0.96	4.01
9	3i	3.34	5.27	5.19	3.30	5.67

Table 13. In silico pharmacokinetic properties and toxicity prediction of the quinoxaline derivatives as well as standard drugs.

S. No	Compound	Pharmaco-kinetics Properties							
		GI Absorption	BBB Permeant	P-gp Substrate	CYP1A2 Inhibitor	CYP2C19 Inhibitor	CYP2C9 Inhibitor	CYP2D6 Inhibitor	CYP3A4 Inhibitor
1	3a	High	Yes	No	Yes	Yes	Yes	No	Yes
2	3b	High	Yes	Yes	Yes	Yes	No	Yes	Yes
3	3c	High	Yes	Yes	Yes	Yes	Yes	No	Yes
4	3d	High	Yes	Yes	Yes	Yes	No	No	No
5	3e	High	Yes	Yes	Yes	Yes	No	No	No
6	3f	High	No	Yes	Yes	Yes	No	No	Yes
7	3g	High	No	No	No	No	No	No	No
8	3h	High	No	No	Yes	Yes	No	No	No
9	3i	High	No	No	No	Yes	Yes	No	No

adherence to Lipinski's Rule of Five, and a bioavailability score of 0.55. Since all of the generated compounds exhibited good drug-likeness properties and no deviations from the Lipinski's rule of five, they may be considered appropriate for drug processing. Their profiles are comparable to other quinoxaline-based compounds reported in the literature, suggesting their potential as drug candidates for peripheral-targeted therapies.[73]

Table 15. Comparison of the present method with literature reports for the synthesis of similar compounds.

S. No.	Catalyst	Reaction Conditions	Time (h)	Yield (%)
1	Acetic acid	Ethanol, reflux	3	82[25]
2	Phthalic acid	Ethanol:H_2O, reflux	3	88[26]
3	Without catalyst	Methanol, reflux	15 min	98[27]
4	Without catalyst	US/stirring RT	50 s	95[28]
5	Acetic acid	Ethanol, reflux	4	90[29]
6	Acetic acid	Ethanol, reflux	4	85[30]
7	Sulfuric acid/SiO_2 catalyst	Ethylene glycol, RT	3	92[33]
8	Without catalyst	Aq. EtOH 80 °C	3	88[37]
9	Without catalyst	Ethanol, reflux	3	84[70]
10	Without catalyst	Ethanol, RT	*3*	98 (Present work)

Table 14. Antibacterial activity of novel benzoyl indeno quinoxaline derivatives 3(a–i) in millimeter (mm).

S. No.	Compounds	*E. Coli*			*S. aureus*			*Klebsiella*		
		10 µL	20 µL	30 µL	10 µL	20 µL	30 µL	10 µL	20 µL	30 µL
1	3a	4	5	4	3	3	3	5	5	5
2	3b	2	2	2	1	1	1	3	3	3
3	3c	Nil	Nil	Nil	Nil	Nil	Nil	1	1	1
4	3d	Nil	Nil	Nil	1	1	4	Nil	Nil	Nil
5	3e	Nil	Nil	Nil	Nil	Nil	Nil	Nil	Nil	Nil
6	3f	Nil	Nil	Nil	5	5	6	Nil	Nil	Nil
7	3g	Nil	Nil	Nil	Nil	Nil	Nil	Nil	Nil	Nil
8	3h	Nil	Nil	Nil	Nil	Nil	Nil	15	15	15
9	3i	2	2	2	Nil	Nil	Nil	4	3	3
10	*Streptomycin* standard	15			15			15		

Streptomycin (25 µg/mL in DMSO) was used as the standard reference drug.

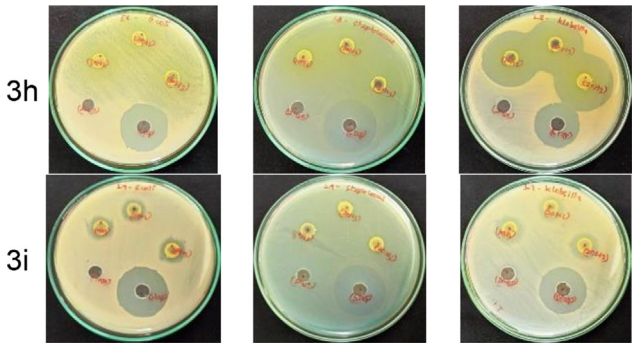

Figure 11. Best Antibacterial activity of the quinoxaline derivatives (3h and 3i) against *E. coli*, *S. aureus*, and *K. pneumoniae*.

4.4. Anti-bacterial Activity

The newly synthesized benzoyl indenoquinoxaline derivatives 3(a–i) exhibited a varying pattern of inhibition against the tested microorganisms which are shown in Table 14. *K. pneumoniae* showed the highest zone of inhibition, while *S. aureus* and *E. coli* exhibited the lowest zone of inhibition. Compounds **3h** and **3i** from the series showed excellent antibacterial activity against *K. pneumoniae*, while the remaining compounds showed moderate antibacterial activity against all tested bacterial strains, including *K. pneumoniae, E. coli*, and *S. aureus* (Figure 11). From the above results it can be inferred that by altering the appropriate R in the benzoyl indenoquinoxaline derivatives it may lead to a promising antibacterial agent (Figure S38). Electron-withdrawing groups (Cl, NO_2) at the *para* or *meta* position (3c, 3d,) enhance antimicrobial activity, likely by increasing membrane permeability or affecting microbial enzymes. Increasing the polarity of substituents (OH, NO_2) tends to improve antimicrobial activity but might reduce penetration through Gram-negative bacterial membranes. Halogenation (Cl) improved activity across both bacterial types, likely due to enhanced lipophilicity aiding cell wall penetration.[74,75]

The synthesis of the title compounds presents more advantages compared to the reports already found in the literature in such a way that the reaction is possible under room temperature instead of those at higher temperatures (Table 15). The time consumed and the % yield of the products also show the superiority of the present protocol. These improvements not only align with green chemistry principles but also demonstrate enhanced sustainability and operational simplicity. The studied compounds exhibited an enhanced zone of inhibition compounds to our previous work.[70]

5. Conclusion

An efficient and convenient synthesis of benzoyl-11*H*-indeno[1,2-*b*]quinoxaline and quinazoline derivatives under catalyst free condition has been achieved. The present method has notable advantages such as, one step method using broad scope, simple separation of the product and green solvent conditions without any chromatographic techniques. In this present study, functionalized derivatives of benzoyl indenoquinoxaline were successfully synthesized. The structure of the compounds **3a** and **3f** were confirmed by the X-ray diffraction method, and the band distance, bond angles, and NMR spectral data were compared with theoretical values by DFT methods. Moreover, these compounds have been examined by molecular docking studies and ADME studies that showed more effective binding with protein 4HJO. From antibacterial studies, the compound **3h** was found to have high antibacterial activity.

Supporting Information

Compound (3a) CCDC: 2366306 (https://doi.org/10.5517/ccdc.csd.cc2kfbgt) and (3f) 2366112 (https://doi.org/10.5517/ccdc.csd.cc2kf46c) contain the supplementary crystallographic data for this paper. These data can be obtained free of charge via http://www.ccdc.cam.ac.uk/conts/retrieving.html (or from the Cambridge Crystallographic Data Centre, 12, Union Road, Cambridge CB21EZ, UK; fax: +44 1223 336033) or E-mail: deposit@ccdc.cam.ac.uk.

Author Contributions

V.R.: Conceptualization; methodology; software; validation; investigation; resources; writing—original draft. **M.K.**: Software; validation; formal analysis; visualization. **K.B.S.**: Investigation; writing and editing. **A.L.**: Conceptualization; validation; investigation; writing—review and editing; supervision; project administration.

Acknowledgments

The authors gratefully acknowledges CIMF (Centre for Instrumentation and Maintenance Facility), RUSA & DST-FIST funded X-ray diffraction facility for X-ray intensity data collection (Periyar University) and also acknowledges NMR Facility, The Gandhigram Rural Institute (Deemed to be university) Gandhigram, Dindigul, Tamil Nadu. We also acknowledge NMR facility, CIC, Bharathiar University supported by DST (PURSE Phase II programme), New Delhi.

Conflict of Interests

The authors declare no conflict of interest.

Data Availability Statement

The data that support the findings of this study are available from the corresponding author upon reasonable request.

Keywords: Antibacterial activity · Benzoyl indenoquinoxaline derivatives · Density functional theory · Molecular docking · Single-crystal-XRD

[1] J. Yamaguchi, A. D. Yamaguchi, K. Itami, *Angew. Chem., Int. Ed.* **2012**, *51*, 8960–9009..
[2] K. Muller, C. Faeh, F. Diederich, *Science* **2007**, *317*, 1881–1886.
[3] C. Vaxelaire, P. Winter, M. Christmann, *Angew. Chem., Int. Ed.* **2011**, *50*, 3605–3607.
[4] H. Roder, N. Krause, *Angew. Chem., Int. Ed.* **2004**, *43*, 1196–1216.
[5] T. Tanaka, A. Enomoto, S. Furukawa, K. Fujita, *Catalysts* **2021**, *11*, 1200.
[6] S. B. Wadavrao, R. S. Ghogare, A. V. Narsaiah, *Org. Commun.* **2013**, *6*, 23–30.
[7] A. A. Abu-Hashem, *Am. J. Org. Chem.* **2015**, *5*, 14–56.
[8] P. Shanmugam, B. Viswambharan, S. Madhavan, *Org. Lett.* **2007**, *9*, 4095–4098.
[9] H. P. Deng, Y. Wei, M. Shi, *Org. Lett.* **2011**, *13*, 3348–3351.
[10] S. M. Anil, R. Shobith, K. R. Kiran, T. R. Swaroop, N. Malleshab, M. P. Sadashiva, *New J. Chem.* **2019**, *43*, 182–187.
[11] B. Karami, S. Khodabakhshi, *J. Chil. Chem. Soc.* **2013**, *581655*–1658.
[12] P. T. Anastas, J. C. Warner, *Green Chemistry: Theory and Practice*, Oxford, New York **1998**, https://doi.org/10.1093/oso/9780198506980.001.0001.
[13] P. T. Anastas, and T. Williamson, G. Chemistry, *Frontiers in Benign Chemical Synthesis and Procedures Oxford*, Oxford University Press, New York **1998**.
[14] A. K. Nezhad, A. Zare, A. H. A. Parhami, A. R. Moosavi Zare, *J. Iran. Chem. Soc.* **2008**, *5*, S40–S46.
[15] B. Ganley, G. Chowdhury, J. Bhansali, J. S. Daniels, K. S. Gates, *Bioorg. Med. Chem.* **2001**, *9*, 2395–2401.
[16] D. Benitez, M. Cabrera, P. Hernández, L. Boiani, M. L. Lavaggi, R. Di Maio, G. Yaluff, E. Serna, S. Torres, M. E. Ferreira, N. Vera de Bilbao, E. Torres, S. Pérez-Silanes, B. Solano, E. Moreno, I. Aldana, A. López de Ceráin, H. Cerecetto, M. González, A. Monge, *J. Med. Chem.* **2011**, *54*, 3624–3636.
[17] G. Aguirre, H. Cerecetto, R. Di Maio, M. González, M. E. Alfaro, A. Jaso, B. Zarranz, M. A. Ortega, I. Aldana, A. Monge-Vega, *Bioorg. Med. Chem. Lett.* **2004**, *14*, 13835–3839.
[18] H. M. A. El-Wahy, *Tetrahedron* **2000**, *56*, 897–907.
[19] P. Ramalingam, S. Ganapaty, B. Rao, *Bioorg. Med. Chem. Lett.* **2010**, *20*, 406–408.
[20] A. S. Khosarkar, D. B. Shinde, *Bioorg. Med. Chem. Let.* **2006**, *16*, 6181–6184.
[21] B. Obot, N. O. Egbedi, *Mater. Chem. Phys.* **2010**, *122*, 325–328.
[22] B. Karami, S. Khodabakhshi, *J. Chil. Chem. Soc.* **2013**, *58*, 1655–1658.
[23] V. Elumalai, J. H. Hansen, *SynOpen* **2021**, *5*, 43–48.
[24] D. Singh, S. Sharma, I. K. M. Kumar, R. Shankar, S. K. Pandey, V. Singh, *Org. Biomol. Chem.* **2019**, *17*, 835–844.
[25] Y. Li, Q. Peng, S. Li, Y. Cai, B. Zhang, K. Sun, J. Ma, C. Yang, H. Hou, H. Su, K. Li, *Chemical* **2019**, *301*, 127–139.
[26] S. Sajjadifar, S. Miri, *Int. J. Chemtech. Res.* **2014**, *6*, 5433–5440.
[27] Y. Kaya, S. Kaya, A. Berisha, A. Ercag, *J. Mol. Struct.* **2023**, *1291*, 135973.
[28] A. Mishra, S. Singh, M. A. Quraishi, V. Srivastava, *Org. Prep. Proced. Int.* **2019**, *51*, 345–356.
[29] D. N. Kanekar, S. S. Dhanawade, A. B. Jadhav, M. Ghadiyali, S. Chacko, R. M. Kamble, *Monatsh. Chem.* **2022**, *153*, 895–906.
[30] H. S. N. Prasad, A. P. Ananda, T. N. Lohith, P. Prabhuprasad, H. S. Jayanth, N. B. Krishnamurthy, M. A. Sridhar, L. Mallesha, P. Mallu, *J. Mol. Struct.* **2022**, *1247*, 131333.
[31] V. Nagalakshmi, R. Nandhini, V. Brindha, B. S. Krishnamoorthy, K. Balasubramani, *J. Organomet. Chem.* **2020**, *912*, 121175.
[32] J. Zhang, W. Xia, S. Huda, J. S. Ward, K. Rissanen, M. Albrecht, *Adv. Synth. Catal.* **2021**, *363*, 3121–3126.
[33] M. Bashirzadeh, F. K. Behbahani, *Eur. Chem. Bull.* **2020**, *9*, 33–37.
[34] A. Toscani, C. Hind, M. Clifford, S. H. Kim, A. Gucic, C. Woolley, N. Saeed, K. M. Rahman, J. M. Sutton, D. Castagnolo, *Eur. J. Med. Chem.* **2021**, *213*, 113172.
[35] B. Banerjee, A. Sharma, M. Kaur, A. Singh, A. Priya, *ChemistrySelect* **2024**, *9*, e202304907.
[36] H. Y. Lian, M. Hu, C. H. Liu, Y. Yamauchi, K. C. W. Wu, *Chem. Commun.* **2012**, *48*, 5151.
[37] N. Vinoth, C. Kalaiarasi, P. Kumaradhas, A. Lalitha, *J. Mol. Struct.* **2021**, *1232*, 130037.
[38] N. Edayadulla, Y. R. Lee, *RSC Adv.*, **2014**, *4*, 11459–11468.
[39] B. S. Krishnamoorthy, A. Thakur, K. K. V. Chakrahari, S. K. Bose, P. Hamon, T. Roisnel, S. Kahlal, S. Ghosh, J. F. Halet, *Inorg. Chem.* **2013**, *51*, 10375–10383.
[40] N. Arumugam, S. M. Soliman, V. Viswanathan, A. I. Almansour, R. S. Kumar, S. M. Mahalingam, B. S. Krishnamoorthy, N. Dege, P. Karuppiah, K. Perumal, *J. Mol. Struct.* **2023**, *1293*, 136189.
[41] R. Nandhini, B. S. Krishnamoorthy, G. Venkatachalam, *J. Organomet. Chem.* **2019**, *903*, 120984.
[42] V. Brindha, B. S. Krishnamoorthy, *Biointerface Res. Appl. Chem.* **2024**, *14*, 73–84.
[43] S. Gomathi, K. Kavitha, N. Savitha, A. Mohana, V. Brindha, B. S. Krishnamoorthy, *Lett. Appl. Nano BioSci.* **2023**, *12*, 1–14.
[44] B. S. Krishnamoorthy, S. Kahlal, S. Ghosh J. F. Halet, *Theor. Chem. Acc.* **2013**, *132*, 1356–1364.
[45] D. D. Perrin, W. L. F. Armarego, *Purification of laboratory chemicals*, 4th ed. Butterworths-Heinemann, London **1996**, 1356–1364.
[46] G. M. Sheldrick, *Acta Crystallogr.* **2015**, *71*, 3–8.
[47] M. Kalidasan, R. Nagarajaprakash, S. Forbes, Y. Mozharivskyj, K. M. Rao, *ZAAC* **2015**, *641*, 715–723.
[48] R. G. Parr, R. A. Donnelly, M. Levy, W. E. Palke, *J. Chem. Phys.* **1978**, *68*, 3801–3807.
[49] R. G. Parr, R. G. Pearson, *J. Am. Chem. Soc.* **1983**, *105*, 7512–7516.
[50] R. G. Parr, P. K. Chattaraj, *J. Am. Chem. Soc.* **1991**, *113*, 1854–1855.
[51] A. I. Almansour, N. Arumugam, S. M. Soliman, B. S. Krishnamoorthy, J. F. Halet, R. Vishnu Priya, J. Suresh, D. M. Althamili, F. A. Alaizari, R. S. Kumar, *J. Mol. Struct.* **2021**, *1237*, 130396.
[52] Z. Zhou, R. G. Parr, *J. Am. Chem. Soc.* **1990**, *112*, 5720–5724.
[53] R. G. Pearson, *Theoretical Models of Chemical Bonding Part II* (Ed: Z. B. Maksic), Springer, Berlin **1990**, p. 45.

[54] J. Luo, Z. Q. Xue, W. M. Liu, J. L. Wu, Z. Q. Yang, *J. Phys. Chem. A* **2006**, *110*, 12005–12009.
[55] P. Forzatti, *Appl. Catal. A* **2001**, *222*, 222–236, https://doi.org/10.1016/S0926-860X(01)00832-8.
[56] C. M. Marian, U. Wahlgren, *Chem. Phys. Lett.* **1996**, *251*, 357–364.
[57] B. A. Hess, C. M. Marian, U. Wahlgren, O. Gropen, *Chem. Phys. Lett.* **1996**, *251*, 365–371.
[58] A. Becke, *Phys. Rev. A* **1986**, *38*, 3098–3100.
[59] F. Neese, *Wiley Interdiscip. Rev. Comput. Mol. Sci.* **2012**, *2*, 73–78.
[60] S. H. Vosko, L. Wilk, M. Nusair, *Can. J. Phys.* **1980**, *58*, 1200–1211.
[61] A. D. Becke, *J. Chem. Phys.* **1986**, *84*, 4524–4529.
[62] J. P. Perdew, *Phys. Rev. B* **1986**, *33*, 8822–8824.
[63] H. Berman, K. Henrick, H. Nakamura, *Nat. Struct. Mol. Biol.* **2003**, *10*, 980.
[64] V. Rajendran, K. Ponnuraj, *J. Biomol. Struct. Dyn.* **2023**, *42*, 10911–10921.
[65] C. Nantasenamat, A. Worachartcheewan, S. Prachayasittikul, N. A. Isarankura, V. Prachayasittikul, *Eur. J. Med. Chem.* **2013**, *69*, 99–114.
[66] E. D. Portakal, Y. Kaya, E. Demirayak, E. K. Yeldir, I. Kaya, *J. Coord. Chem.* **2022**, *75*, 611–628.
[67] E. D. Portakal, Y. Kaya, E. Demirayak, E. K. Yeldir, I. Kaya, *Appl. Organomet. Chem.* **2021**, *35*, 6265–6272.
[68] A. Daina, O. Michielin, V. Zoete, *Sci. Rep.* **2017**, *7*, 1–13.
[69] F. Ameen, P. Srinivasan, T. Selvankumar, S. K. Kannan, S. A. Nadhari, A. Almansob, T. Dawoud, M. Govarthanan, *Bioorg. Chem.* **2019**, *88*, 102970.
[70] G. Sankar, N. Vinoth, N. Nagasundaram, A. Lalitha, *ChemistrySelect* **2022**, *7*, 1–6.
[71] S. Kethireddy, S. Ketha, L. Eppakayala, S. Chithaluri, *J. Chem.* **2022**, *60*, 346–353.
[72] S. Nandi, R. Jamatia, R. Sarkar, F. K. Sarkar, S. Alam, A. K. Pal, *ChemistrySelect* **2022**, *7*, 202201901.
[73] M. J. Deviprasad, B. S. Hemanth, M. B. Shivaswamy, H. S. N. Prasad, S. Sumathi, R. Aswathy, M. A. Sangamesha, A. P. Ananda, H. S. Jayanth, T. N. Lohith, *BioNanoScience* **2024**, *14*, 5106–5121.
[74] S. Genheden, U. Ryde, D. Discovery **2015**, *10*, 449–461.
[75] A. E. El-Samahy, G. A. Ezet Eldeken, E. Mostafa Zayed, F. Hassan Osman, G. Elgemeie, *ChemistrySelect* **2023**, *8*, 202300639.

Manuscript received: June 11, 2025